Journal of Atomic, Molecular, Condensed Matter & Nano Physics
Vol. 8, No. 2, pp. 157–165, 2021
ISSN 2582-8215
Published by RGN Publications

http://www.rgnpublications.com

DOI: 10.26713/jamcnp.v8i2.1671

Research Article

Quantum Optical Analysis of Atomic Density and Refractive Index Employing Cavity Enhanced Absorption Spectroscopy

Surabhi Yadav[1], Suman Dudeja[2] and Aranya B. Bhattacherjee*[1]

[1] *Department of Physics, Birla Institute of Technology and Science, Pilani, Hyderabad Campus, Telangana 500078, India*
[2] *Department of Chemistry, ARSD College* (*University of Delhi*)*, Delhi 110007, India*
***Corresponding author:** aranyabhuti@hyderabad.bits-pilani.ac.in

Received: September 9, 2021 **Accepted:** October 28, 2021

Communicated by: G. Somasundaram

Abstract. We propose a novel cavity enhanced absorption spectroscopic technique to sensitively measure atomic density and refractive index of a sample gas. We theoretically investigate the quantum optical response of a gas of atoms enclosed inside an optical cavity to a probe beam that passes through it. In particular, we study the intracavity spectra, the output spectra and the spectra of the fluctuations. We show that the response of the system is sensitive to small changes in the number of atoms and the refractive index.

Keywords. Quantum optical response, Cavity enhanced absorption spectroscopy, Fluctuation dynamics

PACS. 42.50.-p, 53.20.-t, 33.80.-b, 37.30.+i

1. Introduction

Physical properties of chemicals compounds like refractive index and atomic/molecular density (concentration) are not observed directly but through their effects on a light beam passing through a sample. As a result of the absorption of light passing through the compound, particles are excited to higher energy levels and then lose energy in various ways like spontaneous emission, collision, etc., this forms the basis of absorption spectroscopy. The relationship between

concentration (C), the path length of the sample (l), the incident ($I_0(\lambda)$) and transmitted ($I(\lambda,l)$) intensities of radiation is expressed by the Bear-Lambert Law, $I(\lambda,l) = I_0(\lambda)\exp(-Cl\sigma(\lambda))$, where $\sigma(\lambda)$ is the absorption cross-section [3, 12, 18]. There are many numerous techniques that has been applied to gas detection, identification and measuring its refractive index and density. One of the popular methods is *Differential Optical Absorption Spectroscopy* (DOAS) which has been applied to monitoring atmosphere pollutants [11, 13, 17]. In order to increase the sensitivity, reflective multipass cells are used like *tunable diode laser spectroscopy* (TDLAS) [7, 9]. However, optoelectronic methods provide a better alternative to sensitive measurements of concentration. *Carity Ring Down Spectroscopy* (CRDS) provides a much higher sensitivity compared to conventional absorption spectroscopy [4]. Some of the different types of carity enhanced systems that are in use are Pulsed-CRDS [14], continuous wave-CRDS [8], *integrated cavity output spectroscopy* (ICOS) [10], fiber-optic CRDS [1] and *ring-down spectral photography* (RSP) [6, 15, 16]. Given the interesting applications of optoelectronic techniques in absorption spectroscopy, we theoretically propose and analyse the quantum optical response of a Fabry-Perot cavity being used as a sensitive sensor to measure the refractive index and atomic/molecular density of a gas confined in the optical cavity.

2. The Model and Theory

We consider a gas of N two-level atoms confined in an optical cavity with resonance frequency ω_c as shown in Figure 1. A strong pump field with frequency ω_l drives the cavity. The cavity field interacts with the gas atoms through the Jaynes-Cummings interaction with the coupling strength g. The Hamiltonian of the system can be written as,

$$H = \hbar\omega_c a^\dagger a + \hbar\sum_{i=1}^{N}\omega_d\sigma_{11}^i + \hbar g\sum_{i=1}^{N}(a^\dagger\sigma_-^i + a\sigma_+^i) + i\hbar E_p(a^\dagger e^{-i\omega_l t} - ae^{i\omega_l t}) + i\hbar E_{pr}(a^\dagger e^{-i\omega_p t} - ae^{i\omega_p t}). \tag{2.1}$$

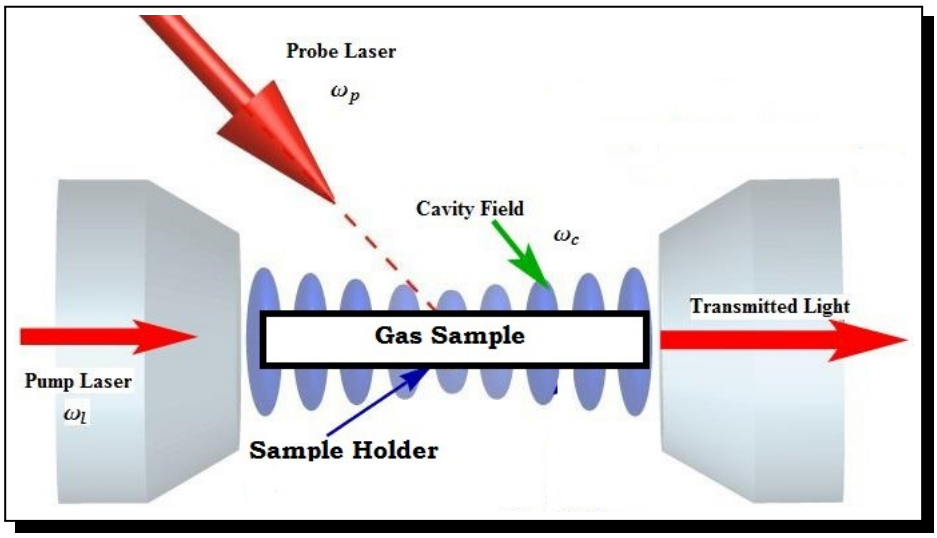

Figure 1. Schematic diagram of the cavity enhanced absorption spectroscopic technique

The first term is the bare energy of the optical cavity with $a(a^\dagger)$ being the destruction (creation) operator of the cavity photon. Here we are taking the ground state $|0\rangle$ energy as zero. Therefore in the second term $\hbar\omega_d$ is the energy of separation between the ground $|0\rangle$ and the first excited state $|1\rangle$, with $\sigma_{11}^i = |1\rangle\langle 1|$. The third term is the Jaynes-Cummings interaction term between the optical cavity mode and two-level atoms, with $\sigma_\pm^i$ are the usual Pauli operators of the i^{th} atom. The fourth term is the pump field driving the cavity with pumping rate E_p and frequency ω_l. The last term is the probe with amplitude E_{pr} and frequency ω_p. We use the Holstein-Primakoff transformation [2] and define $\sum_N^{i=1}\sigma_+^i = \sqrt{N}A^\dagger$, $\sum_N^{i=1}\sigma_-^i = \sqrt{N}A$, where $[A, A^\dagger] = 1$ is satisfied. Now, we rewrite the Hamiltonian of eqn. (2.1) in a frame rotating at the pump frequency ω_l. This yield:

$$H = \hbar\Delta_c a^\dagger a + \hbar\Delta_d A^\dagger A + \hbar g_N(a^\dagger A + aA^\dagger) + i\hbar E_p(a^\dagger - a) + i\hbar E_{pr}(a^\dagger e^{-i\delta t} - ae^{i\delta t}), \tag{2.2}$$

where $\Delta_c = \omega_c - \omega_l$, $\Delta_d = \omega_d - \omega_l$, $\delta = \omega_{pr} - \omega_l$ and $g_N = g\sqrt{N}$.

Using the Hamiltonian of eqn. (2.2), the Heisenberg-Langevin equations for the operators a and A can be written as,

$$\dot{a} = -i(\Delta_c - i\kappa_c/2)a - ig_N A + E_p, \tag{2.3}$$

$$\dot{A} = -i(\Delta_d - i\kappa_d/2)A - ig_N a. \tag{2.4}$$

Here κ_c and κ_d are the decay rates of the cavity mode and the two-level atoms. It is important to note that the decay rate of the cavity photon κ_c is,

$$\kappa_c = \frac{c}{2nLF}, \tag{2.5}$$

where c is the velocity of light, n is the refractive index of the medium, L is the length of the cavity and F is the finesse of the cavity defined as,

$$F = \frac{\pi\sqrt{R}}{1-R}, \tag{2.6}$$

where R is the reflectivity of the mirrors. The lifetime of the photon $\tau_p = 1/\kappa_c$. Larger the refractive index n, longer the time, photon stays inside the cavity. In the next section, we will analyze the steady state solutions of eqns. (2.3) and (2.4) under the mean-field approximation.

3. Steady State Analysis

In the eman-field approximation, $\langle a\rangle = a_s$ and $\langle A\rangle = A_s$. Taking $\langle\dot{a}\rangle = \langle\dot{A}\rangle = 0$, we obtain from the Heisenberg equations of motion the follwing steady-state solutions:

$$A_s = -\frac{g_N a_s}{(\Delta_d - i\kappa_d/2)}, \tag{3.1}$$

$$a_s = -\frac{(g_N A_s + E_p)}{(\Delta_c - i\kappa_d/2)}. \tag{3.2}$$

Solving eqns. (3.1) and (3.2), we get,

$$|a_s|^2 = \frac{|E_p|^2(\Delta_d^2 + \kappa_d^2/4)}{(g_N^2 + \kappa_c\kappa_d/4 - \Delta_c\Delta_d)^2 + (\Delta_d\kappa_c/2 + \Delta_c\kappa_d/2)^2}. \tag{3.3}$$

Figure 2 illustrates the influence of changing the number of atoms N and the refractive index n on the intracavity photon number $|a_s|^2$. Changes in N and n is directly associated

with changes in g_N and κ_c respectively. Figure 2a illustrates intracavity photon number $|a_s|^2$ as a function of Δ_c/κ_c for two values of $g_N = 1.0\kappa_c$ (thick line) and $g_N = 1.5\kappa_c$ (thin line). As evident, for $g_N = 1.5\kappa_c$, the values of $|a_s|^2$ are much lower compared to that for $g_N = 1.0\kappa_c$ since $g_N = 1.5\kappa_c$ has relatively a larger number of atoms, hence leading to a larger absorption of cavity photons. Figure 2b shows the variation of $|a_s|^2$ as a function of g_N/κ_c. A steep decrease in $|a_s|^2$ as g_N/κ_c increases is noticed. Figure 2c demonstrates the variation of $|a_s|^2$ as a function of Δ_c/κ_d for two values of $\kappa_c/\kappa_d = 1.0$ (thick line) and $\kappa_c/\kappa_d = 1.5$ (thin line). Higher value of κ_c indicates a lower refractive index. Clearly, a higher value of n (hence smaller κ_c) diminishes $|a_s|^2$. The intracavity intensity corresponding to $\kappa_c/\kappa_d = 1.5$ is smaller compared to that for $\kappa_c/\kappa_d = 1.0$ since a larger κ_c implies smaller photon lifetime τ_p. Hence, the photon stays inside the cavity for a shorter duration of time. In Figure 2d, plot of $|a_s|^2$ versus κ_c/κ_d shows an almost linear decrease in $|a_s|^2$ as κ_c increases.

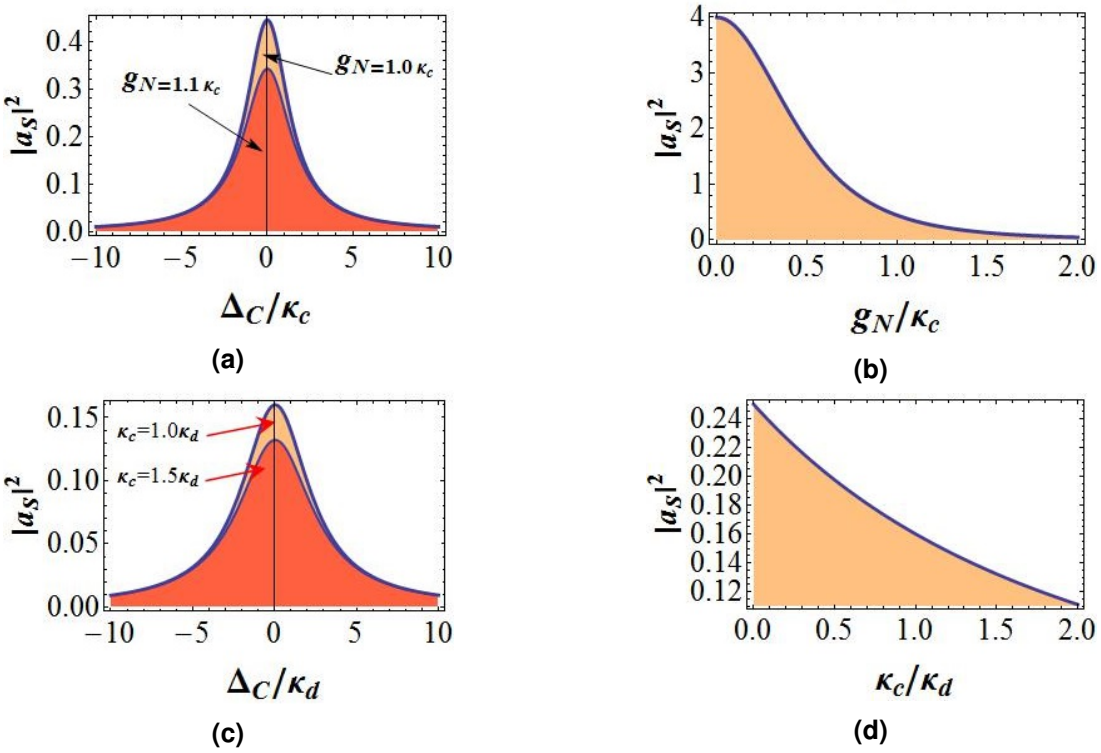

Figure 2. (a) Plot of intracavity photons $|a_s|^2$ as a function of Δ_c/κ_c for two different values of $g_N = 1.0\kappa_c$ (thick line) and $g_N = 1.1\kappa_c$ (thick line), (b) Plot of $|a_s|^2$ as a function of g_N/κ_c, (c) Plot of $|a_s|^2$ versus Δ_c/κ_d for two values of $\kappa_c = 1.0\kappa_d$ (thick line) and $\kappa_c = 1.5\kappa_d$ (thin line), (d) Plot of $|a_s|^2$ versus κ_c/κ_d. All the parameters in plots (a) and (b) are dimensionless with respect to κ_c while in plots (c) and (d), the parameters are dimensionless with respect to κ_d

4. Output Field: Input-Output Theory

In this section, we calculate the output field from the cavity which is related to the input field via the internal dynamics of the cavity [5]. Rewitting eqns. (2.3) and (2.4) in frequency space,

$$-i\omega a(\omega) = -i(\Delta_c - i\kappa_c/2)a(\omega) - ig_N A(\omega) + \sqrt{\kappa_c}a_{in}(\omega), \tag{4.1}$$

$$-i\omega A(\omega) = -i(\Delta_d - i\kappa_d/2)A(\omega) - ig_N a(\omega). \tag{4.2}$$

Here, we have replaced E_p by $\sqrt{\kappa_c}a_{in}(\omega)$, where $a_{in}(\omega)$ describes the incoming field in frequency space. Solving eqns. (4.1) and (4.2) and using the input-output relation $a_{out}(\omega) = a_{in}(\omega) - \sqrt{\kappa_c}a(\omega)$, where $a_{out}(\omega)$ is the output field yields $a_{out}(\omega)$ as,

$$a_{out}(\omega) = \frac{f_N(\omega)a_{in}(\omega)}{f_D(\omega)}, \tag{4.3}$$

where $f_N(\omega) = \left(g_N^2 - \kappa_c\kappa_d/4 - (\Delta_c - \omega)(\Delta_d - \omega)\right) + i\left((\Delta_c - \omega)\kappa_d/2 - (\Delta_d - \omega)\kappa_c/2\right)$ and $f_D(\omega) = \left(g_N^2 + \kappa_c\kappa_d/4 - (\Delta_c - \omega)(\Delta_d - \omega)\right) + i\left((\Delta_d - \omega)\kappa_c/2 - (\Delta_c - \omega)\kappa_d/2\right)$.

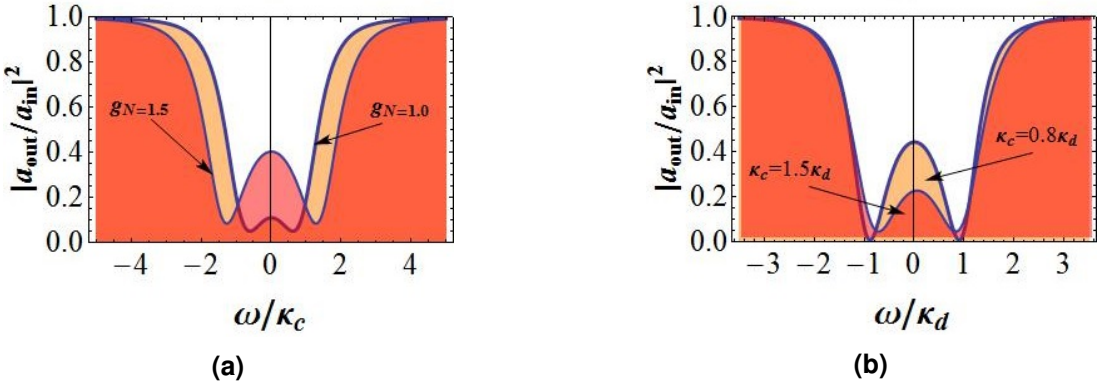

Figure 3. (a) Plot of output field $|\frac{a_{out}(\omega)}{a_{in}(\omega)}|^2$ as a function of ω/κ_c for $g_N = 1.0\kappa_c$ (thick line) and $g_N = 1.5\kappa_c$ (thin line), (b) plot of $|\frac{a_{out}(\omega)}{a_{in}(\omega)}|^2$ versus ω/κ_c for $\kappa_c = 0.8\kappa_d$ (thick line) and $\kappa_c = 1.5\kappa_d$ (thin line). All the parameters in plot (a) are dimensionless with respect to κ_c while in plot (b), the parameters are dimensionless with respect to κ_d

Figure 3 illustrates the plot of eqn. (4.3) as a function of ω/κ_c. In Figure 3a, plot of $|\frac{a_{out}(\omega)}{a_{in}(\omega)}|^2$ as a function of ω/κ_c for $g_N = 1.0\kappa_c$ (thick line) and $g_N = 1.5\kappa_c$ (thin line) is shown. Two symmetrical absorption dips are visible around $\omega/\kappa_c = 0$ for $g_N = 1.0\kappa_c$. The separation between the two absorption dips increase on increasing $g_N = 1.5\kappa_c$. A small transmission seen at $\omega = 0$ for $g_N = 1.0\kappa_c$ also significantly increases for $g_N = 1.5\kappa_c$. The separation between the two absorption dips increases as g_N (hence N) increases. Figure 3b illustrates the variation of $|\frac{a_{out}(\omega)}{a_{in}(\omega)}|^2$ as a function of ω/κ_d for two values of $\kappa_c = 0.8\kappa_d$ (thick line) and $\kappa_c = 1.5\kappa_d$ (thin line). The separation between the absorption dips is not significantly differ for the two different values of κ_c but the transmission at $\omega = 0$ is higher for $\kappa_c = 0.8\kappa_d$ compared to that for $\kappa_c = 1.5\kappa_d$. This indicates a higher absorption of input light for a larger refractive index as was also evident from Figure 2d.

5. Absorption Spectra: Fluctuation Dynamics

Compared to the strong pump field, the probe field is weak that satisfies the condition $E_{pr} \ll E_p$. We can therefore linearize the dynamical equations of the system by considering $a = a_s + \delta a$ and $A = A_s + \delta A$. Here a_s and A_s are the average steady state values of a and A respectively while δa and δA are their corresponding fluctuations. Therefore, the *Quantum Langevin Equation*

(QLE) are:

$$\dot{\delta a} = -i(\Delta_c - i\kappa_c/2)\delta a - ig_N\delta A + E_{pr}e^{-i\delta t} + f_{in}, \tag{5.1}$$

$$\dot{\delta A} = -i(\Delta_d - i\kappa_d/2)\delta A - ig_N\delta a, \tag{5.2}$$

where f_{in} is the noise term for δa, satisfying $\langle f_{in} = 0\rangle$. The fluctuation terms δa, δA and the noise term f_{in} can be rewritten as [19],

$$\delta a = \delta a_+ e^{-i\delta t} + \delta a_- e^{i\delta t}, \tag{5.3}$$

$$\delta A = \delta A_+ e^{-i\delta t} + \delta A_- e^{i\delta t}, \tag{5.4}$$

$$f_{in} = \delta f_{in,+} e^{-i\delta t} + \delta f_{in,-} e^{i\delta t}. \tag{5.5}$$

Substituting eqns. (5.3) to (5.5) in eqns. (5.1) and (5.2) yields the equations for the components δa_+ and δA_+ as,

$$\dot{\delta a_+} = (i\lambda_a - \kappa_c/2)\delta a_+ - ig_N\delta A_+ + E_{pr} + \delta f_{in,+}, \tag{5.6}$$

$$\dot{\delta A_+} = (i\lambda_A - \kappa_d/2)\delta A_+ - ig_N\delta a_+, \tag{5.7}$$

where $\lambda_a = \delta - \Delta_c$ and $\lambda_A = \delta - \Delta_d$. Under the mean-field steady state condition $\langle \dot{\delta a_+}\rangle = \langle \dot{\delta A_+}\rangle = 0$, we obtain

$$0 = (i\lambda_a - \kappa_c/2)\langle \delta a_+\rangle - ig_N\langle \delta A_+\rangle + E_{pr}, \tag{5.8}$$

$$0 = (i\lambda_A - \kappa_d/2)\langle \delta A_+\rangle - ig_N\delta\langle a_+\rangle. \tag{5.9}$$

The solution of $\langle \delta a_+\rangle$ is obtained as,

$$\langle \delta a_+\rangle = \frac{E_{pr}}{(\kappa_c/2 - i\lambda_a) + \frac{g_N^2}{(\kappa_d/2 - i\lambda_A)}}. \tag{5.10}$$

Using the input-output relation of the cavity, we obtain the quadrature ϵ_T of the output field as,

$$\epsilon_T = \frac{2\kappa_c\langle \delta a_+\rangle}{E_{pr}} = \frac{2\kappa_c}{(\kappa_c/2 - i\lambda_a) + \frac{g_N^2}{(\kappa_d/2 - i\lambda_A)}}. \tag{5.11}$$

The real part $Re[\epsilon_T]$ describe the absorption of the system in which we are interested. Figure 4 shows the plot of $Re[\epsilon_T]$ versus δ/κ_c (Figure 4a and Figure 4b) and δ/κ_d (Figure 4c). Figure 4a for $g_N = 1.0\kappa_c$ shows a typical plot with two symmetrical absorption peaks around both sides of $\delta = 0$ and a small transparency dip at $\delta = 0$. At $g_N = 2.0\kappa_c$, the separation between the absorption peaks increases with a corresponding decrease in amplitude of $Re[\epsilon_T]$. The transparency dip also increases at $\delta = 0$ for $g_N = 2.0\kappa_c$. Figure 4b shows the effect of Δ_c on the $Re[\epsilon_T]$. For very small $\Delta_c = 0.01\kappa_c$, a symmetrical spectrum around $\delta = 0$ is obtained. Asymmetry in the absorption spectrum is generated as soon as Δ_c deviates significantly from $\Delta_c = 0$ (here we have taken $\Delta_c = 1.2\kappa_c$). Figure 4c shows the variation of $Re[\epsilon_T]$ as a function of δ/κ_d for two values of $\kappa_c : \kappa_c = 0.8\kappa_c$ and $\kappa_c = 1.5\kappa_d$. At higher value of κ_c $(= 1.5\kappa_d)$, the absorption is more compared to that for $\kappa_c = 0.8\kappa_d$. This is evident from the plots that the amplitude (dip) of the absorption peaks (transparency) is more (less) for $\kappa_c = 1.5\kappa_d$ compared to that for $\kappa_c = 0.8\kappa_c$. A larger κ_c implies a smaller lifetime of the photon τ_p inside the cavity. Consequently, for a larger $\kappa_c = 1.5\kappa_d$, the output intensity is greater as compared to that for a relatively smaller $\kappa_c = 0.8\kappa_d$.

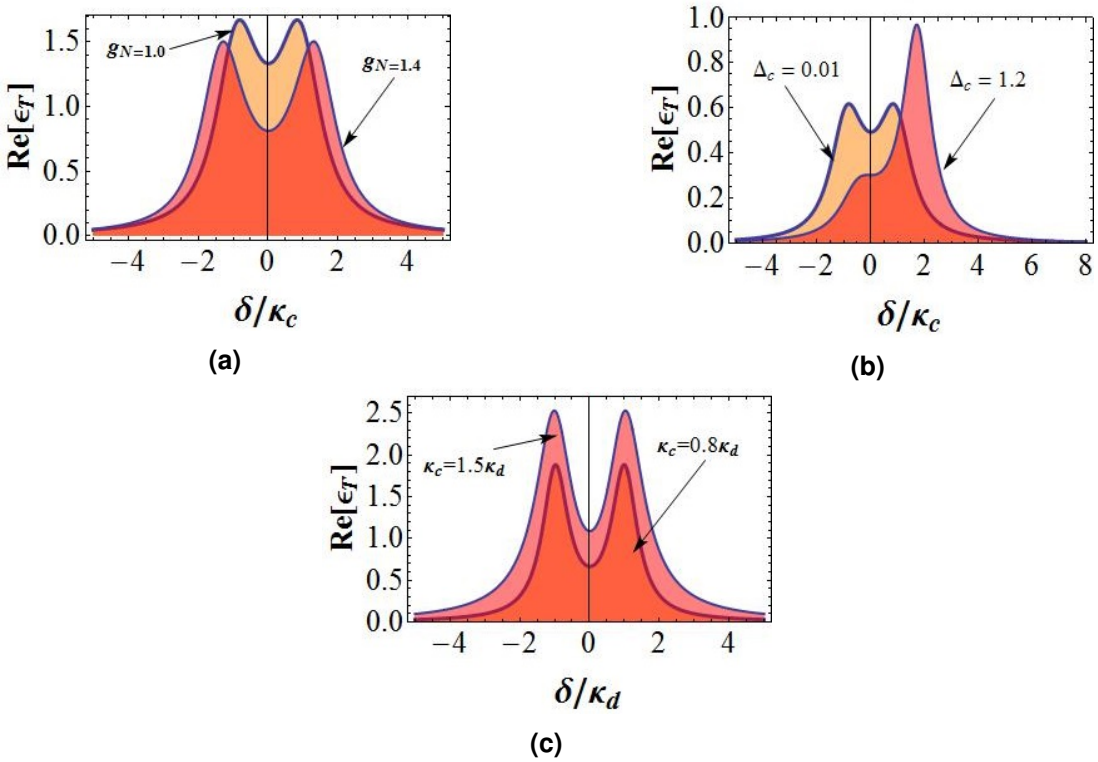

Figure 4. (a) Absorption spectrum $Re[\epsilon^T]$ as a function of δ/κ_c for $g_N = 1.0\kappa_c$ (thick line) and $g_N = 1.4\kappa_c$ (thin line), (b) $Re[\epsilon^T]$ as a function of δ/κ_c for two values of cavity detuning $\Delta_c = 0.01\kappa_c$ (thick line) and $\Delta_c = 1.2\kappa_c$ (thin line), (c) Plot of $Re[\epsilon^T]$ as a fucntion of δ/κ_d for $\kappa_c = 0.8\kappa_d$ (thick line) and $\kappa_c = 1.5\kappa_d$ (thin line). All the parameters in plots (a) and (b) are dimensionless with respect to κ_c while in plot (c), the parameters are dimensionless with respect to κ_d

6. Conclusions

In this work, quantum optical analysis of cavity enhanced absorption spectroscopic method was shown. This method provide the possibility of a greater level of sensitivity compared to conventional absorption spectroscopy. Multiple transits of the intracavity laser field through the sample between the two cavity mirrors allow for a larger atom-field interaction leading to an increased sensitivity of the proposed technique. A small change in the number of atoms or the refractive index can be detected with precision particularly when one is measuring the fluctuation spectra. In practical implementations, a single mode stabilized pump laser, a weak probe laser which can be derived from the pump, a high quality factor optical cavity and a very sensitive photoreceiver is required.

Acknowledgement

Surabhi Yadav acknowledges BITS, Pilani, Hyderabad Campus for the PhD fellowship.

Competing Interests

The authors declare that they have no competing interests.

Authors' Contributions

All the authors contributed significantly in writing this article. The authors read and approved the final manuscript.

References

[1] K. Atherton, G. Stewart and B. Culshaw, Gas detection by cavity ringdown absorption with a fiber optic amplifier loop, *Proceedings SPIE 4577, Vibrational Spectroscopy-based Sensor Systems* **4577** (2002), 25 – 31, DOI: 10.1117/12.455741.

[2] Q. He, F. Badshah, T. Alharbi, L. Li and L. Yang, Normal-mode splitting in a linear and quadratic optomechanical system with an ensemble of two-level atoms, *Journal of the Optical Society of America B* **37** (2020), 148 – 156, DOI: 10.1364/JOSAB.37.000148.

[3] C. N. Banwell and E. M. McCsah, *Fundamentals of Molecular Spectroscopy*, 4th edition, McGraw Hill Education (India) Pvt. Ltd., Chennai (2018).

[4] K. W. Busch and M. A. Busch, *Cavity-Ringdown Spectroscopy*, ACS Symposium series, American Chemical Society, Washington DC (1999), DOI: 10.1021/bk-0720.

[5] M. J. Collett and C. W. Gardiner, Squeezing of intracavity and traveling-wave light fields produced in parametric amplification, *Physical Review A* **30** (1984), 1386 – 1391, DOI: 10.1103/PhysRevA.30.1386.

[6] A. Czyżewski, S. Chudzyński, K. Ernst, G. Karasiński, L. Kilianek, A. Pietruczuk, W. Skubiszak, T. Stacewicz, K. Stelmaszczyk, B. Koch and P. Rairoux, Cavity ring-down spectrography, *Optics Communications* **191** (2001), 271 – 275, DOI: 10.1016/S0030-4018(01)01134-8.

[7] J.-F. Doussin, R. Dominique and C. Patrick, Multiple-pass cell for very-long-path infrared spectrometry, *Applied Optics* **38** (1999), 4145 – 4150, DOI: 10.1364/ao.38.004145.

[8] Y. He and B. J. Orr, Ringdown and cavity-enhanced absorption spectroscopy using a continuous-wave tunable diode laser and a rapidly swept optical cavity, *Chemical Physics Letters* **319** (2000), 131 – 137, DOI: 10.1016/S0009-2614(00)00107-X.

[9] C. V. Horii, M. S. Zahniser, D. D. Nelson, J. B. McManus and S. C. Wofsy, Nitric acid and nitrogen dioxide flux measurements: A new application of tunable diode laser absorption spectroscopy, *Proceedings of SPIE – The International Society for Optical Engineering* **3758** (1999), 152 – 161, DOI: 10.1117/12.366448.

[10] V. L. Kasyutich, C. E. Canosa-Mas, C. Pfrang, S. Vaughan and R. P. Wayne, Off-axis continuous-wave cavity-enhanced absorption spectroscopy of narrow-band and broadband absorbers using red diode lasers, *Applied Physics B* **75** (2002), 755 – 761, DOI: 10.1007/s00340-002-1032-3.

[11] R. V. Martin, D. D. Parrish, T. B. Ryerson, Jr. D. K. Nicks, K. Chance, T. P. Kurosu, D. J. Jacob, E. D. Sturges, A. Fried and B. P. Wert, Evaluation of GOME satellite measurements of tropospheric NO_2 and HCHO using regional data from aircraft campaigns in the southeastern United States, *Journal of Geophysical Research* **109**(D24) (2004), 1 – 11, DOI: 10.1029/2004JD004869.

[12] D. Meschede, *Optics, Light and Lasers*, Wiley-VCH (2007).

[13] S. Noël, H. Bovensmann, J. P. Burrows, J. Frerick, K. V. Chance and A. H. P. Goede, Global atmospheric monitoring with SCIAMACHY, *Physics and Chemistry of the Earth, Part C: Solar, Terrestrial and Planetary Science* **24** (1999), 427 – 434, DOI: 10.1016/S1464-1917(99)00066-5.

[14] A. O'Keefe and D. A. G. Deacon, Cavity ring-down optical spectrometer for absorption measurements using pulsed laser sources, *Review of Scientific Instruments* **59** (1988), 2544 – 2554, DOI: 10.1063/1.1139895.

[15] J. J. Scherer, J. B. Paul, H. Jiao and A. O'Keefe, Broadband ringdown spectral photography, *Applied Optics* **40** (2001), 6725 – 6732, DOI: 10.1364/ao.40.006725.

[16] K. Stelmaszczyk, M. Fechner, P. Rohwetter, M. Queissr, A. Czyzewski, T. Stacewicz and L. Wöste, Towards supercontinuum cavity ringdown spectroscopy, *Applied Physics B* **94** (2009), 396 – 373, DOI: 10.1007/s00340-008-3320-z.

[17] P. Wang, A. Richter, M. Bruns, J. P. Burrows, W. Junkermann, K. P. Heue, T. Wagner, U. Platt and I. Pundt, Airborne multi-axis DOAS measurements of tropospheric SO2 plumes in the Po-valley, Italy, *Atmospheric Chemistry and Physics* **6** (2006), 329 – 338, DOI: 10.5194/acp-6-329-2006.

[18] Weinhein (2007), Optoelectronics: Devices and Application, JacekWojtas (Ed. P. Pradeep, INTECH, Croatia (2019). , DOI: 10.5772/1036.

[19] S.-C. Wu, L.-G. Qin, J. Jing, T. Yan, J. Lu and Z.-Y. Wang, Microwave-controlled optical double optomechanically induced transparency in a hybrid piezo-optomechanical cavity system, *Physical Review A* **98** (2018), 013807, DOI: 10.1103/PhysRevA.98.013807.